

# 3D SPH Simulations of Shocks in Accretion Flows around black holes

G. Gerardi<sup>1</sup> \*, D. Molteni<sup>1</sup> and V. Teresi<sup>1</sup>

<sup>1</sup>*Dipartimento di Fisica e Tecnologie Relative, Università di Palermo, Viale delle Scienze, Palermo, 90128, Italy*

8 December 2018

## ABSTRACT

We present the simulation of 3D time dependent flow of rotating ideal gas falling into a Schwarzschild black hole. It is shown that also in the 3D case steady shocks are formed in a wide range of parameters (initial angular momentum and thermal energy). We therefore highlight the stability of the phenomenon of shock formation in sub keplerian flows onto black holes, and reenforce the role of the shocks in the high luminosity emission from black hole candidates. The simulations have been performed using a parallelized code based on the Smoothed Particles Hydrodynamics method (SPH). We also discuss some properties of the shock problem that allow its use as a quantitative test of the accuracy of the used numerical method. This shows that the accuracy of SPH is acceptable although not excellent.

**Key words:** accretion, accretion disks — black hole physics — hydrodynamics — instabilities

## 1 INTRODUCTION

As Bondi showed in his historical paper (Bondi 1952) the occurrence of shocks in accretion phenomena on compact stellar objects is quite common. Since the radial speed can become supersonic the halting of the flow at a rigid wall leads necessarily to shock formation.

Nevertheless the possibility of radial shock formation around black holes is less obvious since this compact object has no rigid wall. It is true that pre-heating of the infalling gas by radiation from below or other non adiabatic processes can influence the properties of the falling gas and allow shock solutions even in the spherically symmetric regime (Babul et al. 1989).

However, if the gas is falling with some rotation, the centrifugal force can act as a "wall" and therefore trigger the shock formation even in the simple case of ideal gas. This fact was indeed suggested by the excellent pioneer general relativistic simulations of Hawley, Smarr and Wilson (Hawley et al. 1984). The question of the stability of the shock is critically related to the initial angular momentum of the gas, since for large values a standard keplerian disk will be formed, while for low values favorable conditions for standing shocks will occur.

That such shocks can effectively stay at a fixed position has been put forward by S. Chakrabarti (Chakrabarti 1990), see also Chakrabarti (1998). It has been succes-

sively confirmed by the analytical work of Nakayama (Nakayama 1994) and by numerical simulation experiments by Chakrabarti and Molteni (Chakrabarti and Molteni 1993) and following papers. The stability of the shock location is very relevant since, if it is stable, then the shock "engine" is always acting: it is not a transient phenomenon. Further studies, based on numerical simulations in 2D, axis symmetric configurations, revealed different kinds of oscillating behavior over the basic stable regime, see the results in Molteni et al. (1996), Molteni et al. (1996b), Molteni et al. (1999).

Recently the shock scenario has been shown to be very promising also to explain quasi periodic oscillation processes (QPO) occurring in BH candidates (Molteni et al. 2001).

Since all previous studies have been performed in 2D configurations (axial symmetric or in the  $Z=0$  plane), it is natural to investigate the stability of the shocks in full 3D cases. Furthermore we add that this physical problem can be also considered a very critical test in the field of computational fluid dynamics.

The work proceeds as follows: in section 2 we resume the basic physics leading to shock formation and derive a simple formula to obtain the physical parameters necessary to generate the shocks, in section 3 we revise the numerical method and show how a test of any numerical code can be set up and in section 4 we show and discuss the new 3D simulation results.

\* E-mail: gerardi@difter.unipa.it (GG)

## 2 SHOCK FORMATION IN UNVISCOUS SUB-KEPLERIAN FLOWS

Let us resume the very basic physical ingredients of the phenomenon. We suppose that an unviscous gas is falling from very large distance onto a black hole. We will adopt the Paczyński & Wiita potential (Paczyński and Wiita 1980) to mimic the Schwarzschild Black Hole force. It is given by :

$$\Psi(r) = -\frac{GM_\star}{r - r_g} \quad (1)$$

where  $r_g = \frac{2 \cdot G \cdot M}{c^2}$  is the Schwarzschild radius. The basic physical effect can be easily understood in terms of "classical" physics and it is well known that the Paczyński & Wiita force reproduces many relativistic effects with high accuracy.

To obtain the steady state solution we might integrate the differential equations for mass, momentum and energy conservations. In this case one has to start the space integration from the sonic point as explained in the work by Chakrabarti (Chakrabarti 1990). However, in the case of unviscous flow, it is easy to find an algebraic implicit solution, since the total energy is conserved (the Bernoulli theorem) and it can be fairly exploited to close the system of equations and find the solutions.

### 2.1 1D Case

Let us treat first the 1D case. This derivation already appeared in the appendix of Molteni et al. (1999). We repeat here the derivation pointing also to a peculiar aspect of the solution especially relevant to test code accuracy. By 1D we mean that we are in an axially symmetric situation and the disk has no vertical extension ( $v_z = 0$ ,  $Z = 0$ ). Note that the solution is obviously valid *also* in 2D dimensions with  $Z = 0$  (i.e. in the plane XY) if the symmetric condition is maintained. Both in the case of 1D simulations in cylindrical coordinates and in 2D simulations (but with  $Z=0$ ) the difference between the theoretical shock position and the one resulting from simulations depends only on the numerical quality of the code; indeed there is no physical cause intervening to modify the results. Instead, in the 2D or 3D cases (with real vertical extension of the flow), the theoretical procedure to derive the shock position needs the assumption of vertical equilibrium, that, as we will see, is not always satisfied.

We assume also that the accreting gas is ideal (no viscosity and no cooling process is occurring). The angular momentum per unit mass of the flow,  $\lambda$ , must be conserved. In steady state regime we have also conservation of mass given by the equation:

$$\dot{M} = -r \rho v_r = \text{const} \quad (2)$$

Here  $\rho$  is the surface density. In a conservative body force field with a potential  $\Psi(r)$ , also the pressure plays the role of a 'potential' and we have

$$\frac{1}{2}v(r)^2 + \epsilon(r) + \frac{P(r)}{\rho(r)} + \Psi(r) = \frac{1}{2}v(r)^2 + \frac{a(r)^2}{(\gamma - 1)} + \Psi(r) = B \quad (3)$$

Here  $\gamma$  is the adiabatic gas constant,  $B$  is the Bernoulli constant (the thermal energy at infinity),  $a$  is the sound speed  $a = \sqrt{\frac{\gamma \cdot P}{\rho}}$ ,  $\epsilon$  is the internal energy per unit mass,  $v$

is the speed of the flow and  $\lambda$  is the angular momentum, so that  $\frac{1}{2}v^2 = \frac{1}{2}v_\phi^2 + \frac{1}{2}v_r^2 = \frac{\lambda^2}{2r^2} + \frac{1}{2}v_r^2$ .

If the entropy is conserved (no viscosity, no cooling, the presence of the shock will be taken into account few lines below) the polytropic relations are valid,  $P/\rho^\gamma = P_0/\rho_0^\gamma$ , so the relation between the density and sound speed  $\rho = K \cdot a^{2/(\gamma-1)}$ , where  $K = \rho_0/a_0^{2/(\gamma-1)}$ , is also valid.

We have three unknown quantities  $\rho$ ,  $v_r$ ,  $a$ , and three equations. The solutions are functions of  $r$  with angular momentum and Bernoulli constant as parameters determining the specific shape of the solution.

Using the radial Mach number  $m = -\frac{v_r}{a}$ , resolving  $a$  from the Bernoulli relation, and putting all terms in the continuity equation, we have the following implicit solution for the Mach number:

$$\dot{M} = r \cdot m \cdot a \cdot K \cdot a^{\frac{2}{\gamma-1}} \propto f(m) \cdot A(r, B, \lambda)$$

where  $f$  is function only of the mach number:

$$f(m) = \frac{m}{\left[\frac{m^2}{2} + \frac{1}{\gamma-1}\right]^{\frac{\gamma+1}{2(\gamma-1)}}}$$

and  $A$  is function only of  $r$  ( $B$  and  $\lambda$  are parameters) :

$$A(r, B, \lambda) = r [B - V(r, \lambda)]^{\frac{\gamma+1}{2(\gamma-1)}}$$

where

$$V(r, \lambda) = \frac{\lambda^2}{2r^2} - \frac{GM_\star}{r - r_g}$$

is the effective body force potential (gravitational plus centrifugal).

For a given  $\dot{M}$  this equation can be easily solved. The  $f(m)$  function has a single maximum at  $m = 1$ , and it can be inverted both in the subsonic  $0 \leq m < 1$  and supersonic  $m > 1$  regions. The  $A$  function has in general two local minima at  $r_1$  and  $r_2$  with  $r_1 < r_2$ , which can be determined by solving the algebraic equation  $dA/dr = 0$  numerically (high  $\lambda$  values increase the centrifugal barrier and produce minima close to the BH).

At large distances from the BH, the Mach number is  $m \ll 1$ , while close to the horizon it is  $m \gg 1$ . Since the  $f(m) \cdot A(r, B, \lambda)$  product must be constant along the flow, the maximum of  $f(m)$  must be at one of the minima of  $A(r)$ , i.e. at  $r_1$  or  $r_2$ . Therefore we can have two isentropic solutions  $m_1(r)$  and  $m_2(r)$

$$m_{1,2}(r) = f^{-1} \left[ \frac{f(1)A_{\lambda,B}(r_{1,2})}{A_{\lambda,B}(r)} \right] \quad (4)$$

A standing shock can occur in the solution at  $r_{shock}$  if the values  $m_2(r_{shock}) > 1$  and  $m_1(r_{shock}) < 1$  are related by the Hugoniot relation

$$m_1(r_{shock}) = h(m_2(r_{shock})) \quad (5)$$

where the Hugoniot relation for an hypothetical shock at a generic radius is given by

$$h(m_2(r)) = \left[ \frac{2 + (\gamma - 1)m_2(r)^2}{2\gamma m_2(r)^2 - (\gamma - 1)} \right]^{1/2} \quad (6)$$

In general there can be two possible shock positions, but only the outer one is stable as shown by the numerical simulations of Chakrabarti and Molteni

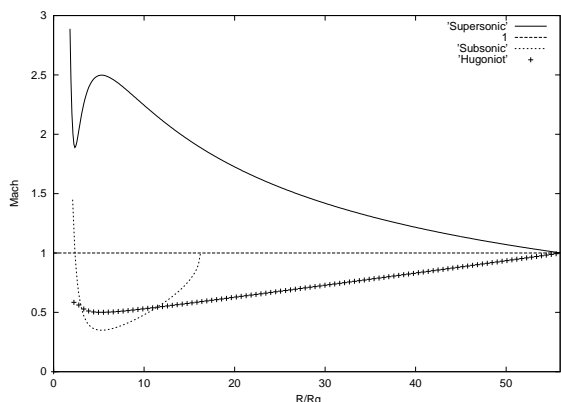


Figure 1. Analytical solution

(Chakrabarti and Molteni 1993) and by the analytical work of Nakayama (Nakayama 1994).

Figure 1 clarifies the procedure for a generic case. The supersonic line corresponds to the  $m_1(r)$  solution while  $m_2(r)$  corresponds to the subsonic branch.

## 2.2 Fictious and true rotation

Let us note that the solution depends on the  $A$  function that contains the term:

$$B - \frac{\lambda^2}{2r^2} + \frac{GM_*}{r - r_g} \quad (7)$$

So, if we give to the flow an angular momentum lower than the theoretical one, but we add an equivalent centrifugal force, the resulting solution does not change. For example, we can obtain the same shock location if we give *no real rotation* to the flow and add to the gravitational force a fictitious force derived from the centrifugal potential  $\frac{\lambda^2}{2r^2}$ , or viceversa, we can inject matter with an extremely fast real rotation, (even super keplerian!) and, at the same time, add a centripetal force.

In this way, playing with real rotation and fictious centrifugal forces we can obtain a variety of solutions with the *same* radial shock position, *same* radial Mach number, *same* density profile. The important point is that the algebraic sum of real and fictious forces must be equal to the force required by the theory. It means that one of the following equations must be satisfied, according to the case

$$\begin{cases} \lambda_{theor}^2 = \lambda_{real}^2 + \lambda_{fict}^2 & \text{if } \lambda_{real} < \lambda_{theor} \\ \lambda_{theor}^2 = \lambda_{real}^2 - \lambda_{fict}^2 & \text{if } \lambda_{real} > \lambda_{theor} \end{cases}$$

where  $\lambda_{theor}$  is the angular momentum value required by the theory to produce a shock at some specified radius. For consistency, if we define the real rotation as a fraction  $f$  of the theoretical one, i.e.  $\lambda_{real} = f \cdot \lambda_{theor}$ , then the fictious force to be added is given by:

$$\begin{cases} \lambda_{fict} = \lambda_{theor} \cdot \sqrt{1 - f^2} & \text{if } f < 1 \\ \lambda_{fict} = \lambda_{theor} \cdot \sqrt{f^2 - 1} & \text{if } f > 1 \end{cases}$$

It is clear that in the fast rotational cases the real shear motion can modify the results due to the numerical viscosity and other numerical code properties: accuracy, conservative structure, etc...

We suggest the possibility to quantify the quality,  $Q$ , of a code as the ratio of the true rotation angular momentum to the theoretical one for which the shock is stable and close to the theoretical position:

$$Q = 1 + \frac{\lambda_{real}}{\lambda_{theor}}$$

The obvious minimum requirement is that a code has  $Q=1$  so that, for no rotation, it produces the shock at the correct position.

## 2.3 2D axis symmetric case

For the 2D case (with real Z extension of the disk) the procedure is similar. We maintain the hypothesis of axial symmetry. We assume that the gas falls down in a condition of vertical equilibrium. Using the same variable names, the mass conservation equation is given by:

$$\dot{M} = -4\pi r H \rho v_r = const \quad (8)$$

where  $H$  is the half thickness of the disk.

The vertical equilibrium hypothesis gives the well known expression for the half disk thickness:

$$H = \frac{\sqrt{GM_* r (r - r_g)} a}{GM_*} \quad (9)$$

The energy equation is still given by:

$$\frac{\lambda^2}{2r^2} + \frac{1}{2}v_r^2 + \epsilon(r) + \frac{P(r)}{\rho(r)} + \Psi(r) = B$$

So again we have three unknown quantities  $\rho$ ,  $v_r$ ,  $a$ , and three equations and we may find the solution exactly in the same way of the 1D case. The difference will be in the exact values of the Mach function and of the geometrical function,  $A(r, \lambda, B)$ , but the shape are very similar: two minima in the geometrical function and one maximum in the Mach function.

The Mach function is now given by:

$$f(m) = \frac{m}{\left[\frac{m^2}{2} + \frac{1}{\gamma-1}\right]^{\frac{\gamma}{\gamma-1}}}$$

and the new  $A$  is function only of  $r$  ( $B$  and  $\lambda$  are parameters):

$$A(r, B, \lambda) = r^{\frac{3}{2}} (r - r_g) [B - V(r, \lambda)]^{\frac{\gamma}{\gamma-1}}$$

where as previously stated

$$V(r, \lambda) = \frac{\lambda^2}{2r^2} - \frac{GM_*}{r - r_g}$$

is the effective body force potential (gravitational plus centrifugal).

## 3 THE PHYSICAL MODEL AND THE NUMERICAL SIMULATIONS

We performed 2D and 3D time dependent simulations of the motion of an ideal gas around a Schwarzschild black hole. The equations we integrate are in the lagrangian formulation ( $\frac{d}{dt}$  is the comoving derivative):

the continuity equation

$$\frac{d\rho}{dt} = -\rho \nabla \cdot \mathbf{v} \quad (10)$$

the momentum equation

$$\frac{d\mathbf{v}}{dt} = -\frac{1}{\rho} \nabla p \quad (11)$$

the energy equation

$$\frac{d\epsilon}{dt} = -\frac{p}{\rho} \nabla \cdot \mathbf{v} \quad (12)$$

the equation of state

$$p = (\gamma - 1)\rho\epsilon \quad (13)$$

Applying the SPH formalism (see Monaghan (1992)), these are transformed into a set of ordinary differential equations (ODEs). These ODEs are subsequently integrated numerically using standard methods. We use the usual summation form for the continuity equation:

$$\rho_i = \sum_{k=1}^N m_k W_{ik} \quad (14)$$

the momentum equation is given by:

$$\frac{d\mathbf{v}_i}{dt} = -\sum_{k=1}^N m_k \left( \frac{p_k}{\rho_k^2} + \frac{p_i}{\rho_i^2} + \Pi_{ik} \right) \cdot \nabla_i W_{ik} \quad (15)$$

the energy equation is:

$$\frac{d\epsilon_i}{dt} = -\sum_{k=1}^N m_k \left( \frac{p_k}{\rho_k^2} + \frac{p_i}{\rho_i^2} + \Pi_{ik} \right) \mathbf{v}_{ik} \cdot \nabla_i W_{ik} \quad (16)$$

Where  $\Pi_{ik}$  is the standard form of the artificial viscosity.

### 3.1 Simulations parameters

Here we show the results of 3D time dependent simulations and add also the results of 2D ( $Z=0$ ) simulations to clarify the item of the code accuracy testing. We focus our attention to a limited set of parameters which predicts a shock position close to the minimum radius allowed (around  $5R_g$ ) (Das et al. 2001). Therefore we are presenting the results concerning two critical cases. However we verified that also for other parameter values the shocks are formed and are stable, in good agreement with the predicted theoretical position. The physical parameters of the cases we discuss here are given in Table 1 and they are well inside the stability region analyzed by Das et al. (2001).

The variables appearing in the Table 1 have the following meaning:  $r_i$  is the inflow radius,  $v_{r_i}$  and  $a_{r_i}$  are the radial speed and sound speed at inflow radius,  $B$  is the Bernoulli constant,  $\lambda$  is the angular momentum per unit mass,  $H$  is the vertical disk thickness at the inflow radius,  $R_{shock}$  is the predicted shock position,  $f$  is the fraction of the real rotation of the gas.

The spatial domain (in cylindrical coordinates) is given by  $r = 0 \div r_i$ ,  $\varphi = 0 \div 2\pi$ ,  $z = -2r_i \div +2r_i$ .

The results have been obtained with a constant value of the spatial resolution  $h$ . This choice gives better results than those ones obtained with variable  $h$ ; we think that the space varying  $h$  option has a larger amount of numerical viscosity

due to the strong jump of  $h$  at the shock location. For 3D runs we used  $h = 0.5$  and  $\gamma = 4/3$ .

The gas particles are injected (with the physical properties given in Table 1) from a set of injection points equally spaced onto the surface of a cylinder of radius  $r_i$  and height  $H$ , which is calculated from the vertical equilibrium assumption. A new particle is injected every time a sphere of radius  $h/2$  around each injector is found to be empty.

### 3.2 Code parallelization

Since our problem doesn't contain self gravitation, we used a spatial domain decomposition to parallelize the SPH code. We show here that this approach is very convenient for the kind of problem we are studying. Our parallel system consists of a biprocessor workstations cluster. As our processors pool has local memory, we use the well known standard: "Message Passing Interface" (MPI) to exchange data. Our physical problem (accretion disks around central star) has a space domain with some degree of central symmetry, so it seems logical to divide the overall domain into sub domains having this type of symmetry. The parallelization paradigm we use is the Multiple Instruction Multiple Data one (MIMD). With this decomposition and paradigms, the code performing the calculations for one sub domain is the standard serial code used for one single domain, with minor modifications. Information exchanges occur always between two consecutive domains.

The three dimensional computational domain is decomposed into concentric cylindrical coronae (sub domains) with centers coincident with the coordinate origin. Figure 2 shows an horizontal cut view, in a case in which the domain is decomposed into four sub domains. All the SPH particles, having vector radius projection (in XY plane) lying between two consecutive cylinders, are assigned to the same sub domain. The number of sub domains is equal or multiple of the number of processors in the cluster.

As the SPH particles have a short-range interaction, only the particles lying within a distance  $\leq 2h$  from the limiting cylinders interact with their analogue particles lying in the previous cylinder or in the next one.

In any moment each processor manages  $n_i$  internal particles plus  $nb_{in}$  edge particles from the inner edge region and  $nb_{out}$  edge particles from the outer edge region.

In each iteration loop the  $n_i$  particle of a sub domain are evolved taking into account the presence of the all  $nb$  particles (for density, pressure forces etc. calculation). Instead the  $nb$  particles are evolved according to the kinematic and dynamic properties they had as internal particles of their original domain. At the end of the time step and before to start the next one a check is performed to verify if some internal particle has migrated into another domain. In this case the particles data are exchanged.

## 4 RESULTS AND DATA ANALYSIS

We show the basic results of the simulations using one panel for each case. In each panel we have 4 figures: the figure top-left shows the number of particles versus time; the figure top-right shows the radial Mach number of all the particles folded, in  $\varphi$ , around the  $z$  axis; the figure bottom-left

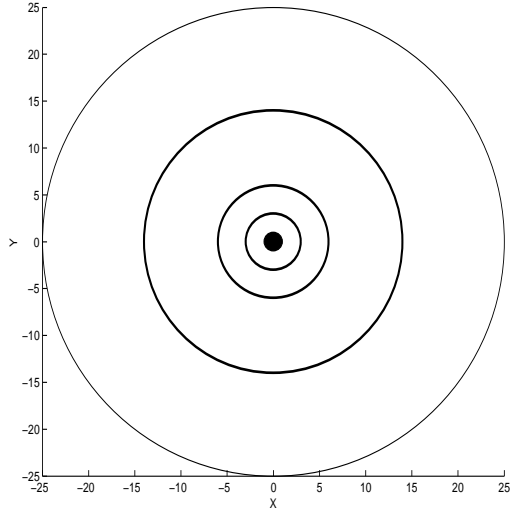


**Figure 2.** domain subdivision

shows the radial speed; the figure bottom-right shows the distribution of the angular momentum of the particles, the scattering of the values is just due to the conservation of the total angular momentum.

As it is clear from Figure 1.1 the system reaches the equilibrium. Figure 1.2, with the folded radial Mach number values, shows that the shock is located at  $R_{shock} = 10.5$ , a position close to the theoretical one ( $R_{shock} = 6.3$ ). A not perfect agreement between the theoretical shock position and the simulation result is not surprising: a discrepancy has to be expected due to the vertical motion of the gas in 3D geometry, while the theory assumes vertical equilibrium (the Mach number profile is also very close to the theoretical one). Figure 1.4 shows that also the mean value of  $\lambda$  is close to the real zero value.

We then simulated the same flow but increasing the amount of true rotation. For a fraction  $f = 0.1$  the flow still reaches the equilibrium state, but the shock is located somewhat outwards compared to the theoretical position.

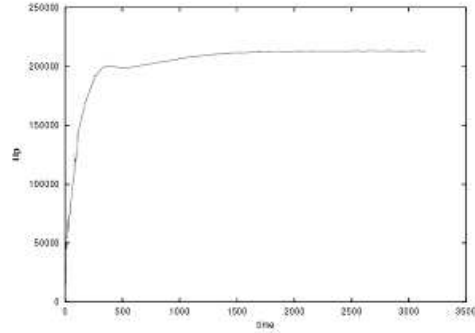
For  $f = 0.2$  the results are shown in Panel 3. The shock is steady, but at a larger radius.

For  $f = 0.4$ , see Panel 4, the system is still in steady state and the shock is further shifted outwards. It is clearly seen that the number of particles versus time is increased.

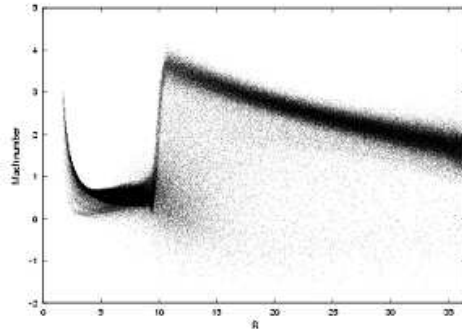
For  $f \geq 0.7$  (not shown) the shock position is unstable: it travels steadily outwards. The number of particles is always increasing. We stopped the simulation before the shock reached the outer boundary of our integration domain.

In general the figures showing the radial speed versus  $r$  point out that, as the true rotation increases, the number of outflowing particles increases. We inject with a fixed angular momentum, but the numerical code viscosity, while conserving the total angular momentum, produces an angular momentum redistribution and therefore the particles with large angular momentum flow away.

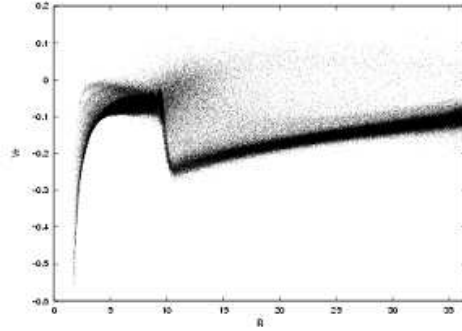
**Panel 1.** Simulation with  $f=0.0$



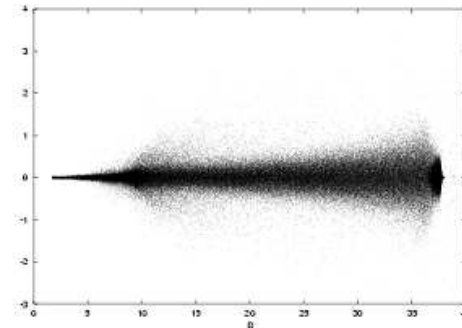
**Figure 1.1** Number of particles versus time



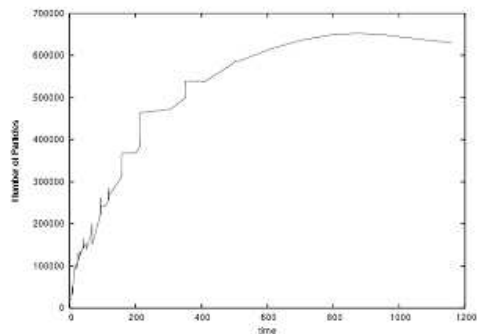
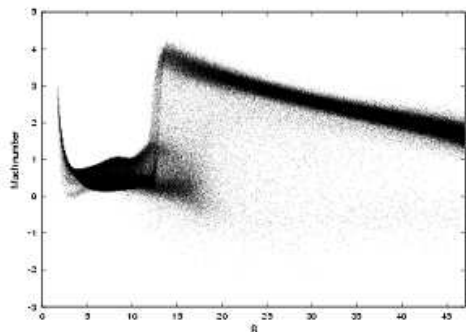
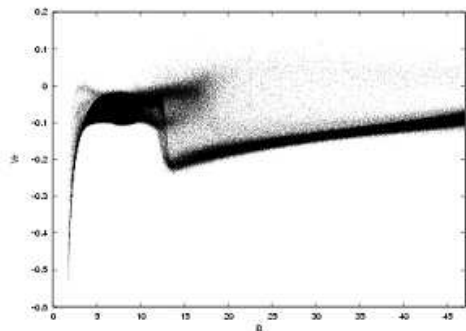
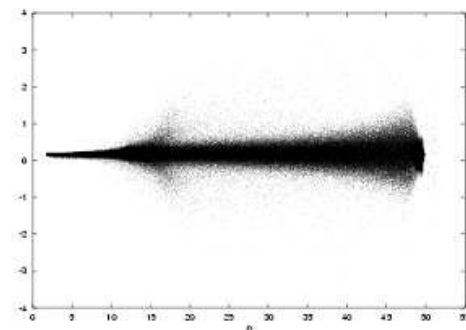
**Figure 1.2** Radial Mach Number versus R



**Figure 1.3** Radial speed versus R



**Figure 1.4** True angular momentum versus R

**Panel 2.** Simulation with  $f=0.1$ **Figure 2.1** Number of particles versus time**Figure 2.2** Radial Mach Number versus R**Figure 2.3** Radial speed versus R**Figure 2.4** True angular momentum versus R

We made also 2D simulations, on the  $Z = 0$  plane. In this case the agreement between the simulation results and the theory should be perfect; the discrepancies are fully attributable to the code properties. We checked that the 2D SPH simulations with different  $f$  values show clearly the effect of the numerical shear viscosity. Panel 5 shows the results obtained with  $f = 0.5$ . The shock is stable. In figure 5.1 the shock position versus time is plotted, in figure 5.2 the radial Mach number (folded in  $\varphi$ ) is plotted versus  $R$ , in figure 5.3 the radial speed (folded in  $\varphi$ ) is displayed and in figure 5.4 the particle distribution in the  $XY$  plane is presented. In this case the agreement between theory and simulation is quite good. Note that the symmetry of the flow is so well conserved that the folded data appear as one dimensional in  $R$ . The physical parameters are  $E = 0.002$ ,  $\lambda = 1.8$ . For gas with  $\gamma = 5/3$  the shock must be  $R_{shock} = 6.78$ , in good agreement with the simulation results. The oscillations in Figure 5.1 are due to the algorithm of the shock identification. The SPH numerical parameters are  $h = 0.2$  and we use  $\alpha = 1$ ,  $\beta = 2$  for the artificial viscosity coefficients. In the case with  $f=0.75$ , here not shown, the shock is still stable, but the position is different from the predicted one. In general, if we compare 2D and 3D simulations with the same parameters and resolution, the 3D case is more stable than the 2D one. We interpret this fact as due to the impossibility of ejecting (along  $Z$ ) high angular momentum gas outside the domain in the 2D case, while in the 3D case the high angular momentum particles are vertically ejected leading to a stabilizing effect.

## 5 CONCLUSIONS

We showed that even in 3D time dependent simulations the standing shocks predicted by Chakrabarti's analysis are formed. In the numerical simulations, for values of the parameters in the theoretical stable zone, the shocks are stable. This fact confirms the relevance of the shock phenomena in accretion flows around black holes in galactic and extragalactic sources. Indeed the standard keplerian disk models around galactic black hole candidates suffer instabilities that make not completely clear the physical scenario. In the case of the extragalactic sources like AGN (active galactic nuclei), supposed to contain black holes, while the keplerian disk can easily take account of the low energy emission, the high luminosity at high energies, X and  $\gamma$ , is still an open problem.

Due to the high CPU cost of 3D simulations the variability properties of the shock flow exhibited in the reduced dimensional simulations (2D in  $r$ - $z$  axis symmetric configuration and 2D  $XY$  plane configuration) will be the subject of a subsequent paper.

We showed also that this physical problem can be used as a test for any fluid dynamics code since it is possible to derive the analytical profile of the solution of the flow and compare it with the simulated one for different degrees of real rotation of the fluid. In this way it is possible to measure the numerical shear viscosity of the code. We show that the 3D SPH code detects the shock at a good level of accuracy.

Panel 3. Simulation with  $f=0.2$

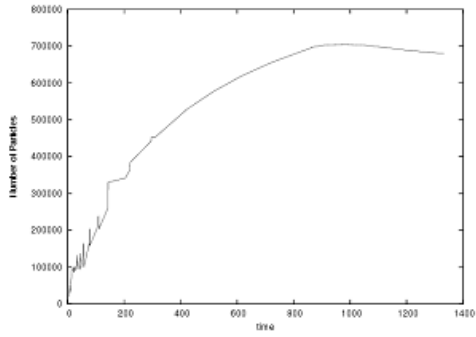


Figure 3.1 Number of particles versus time

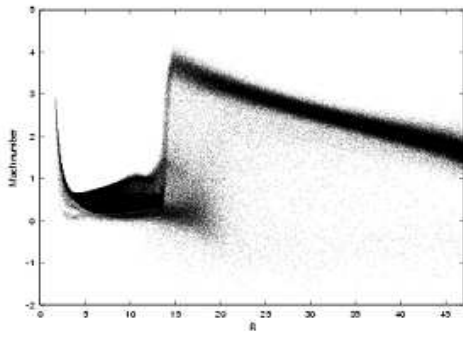


Figure 3.2 Radial Mach Number versus R

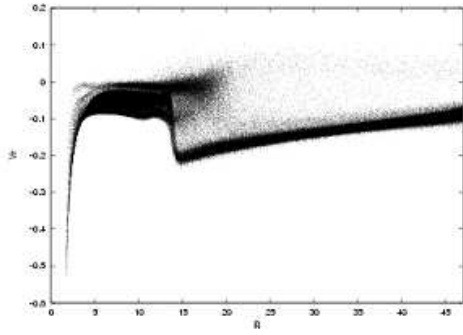


Figure 3.3 Radial speed versus R

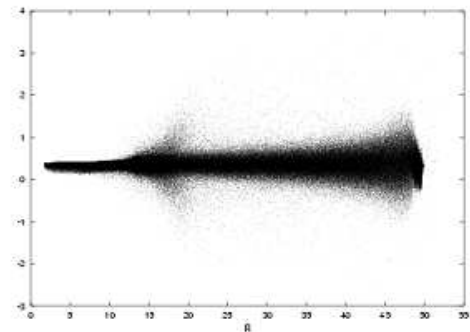


Figure 3.4 True angular momentum versus R

Panel 4. Simulation with  $f=0.4$

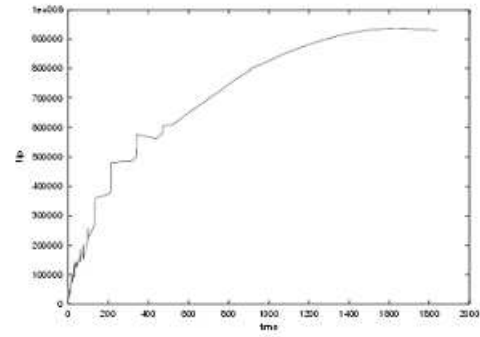


Figure 4.1 Number of particles versus time

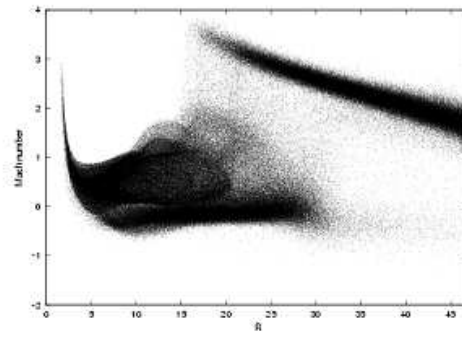


Figure 4.2 Radial Mach Number versus R

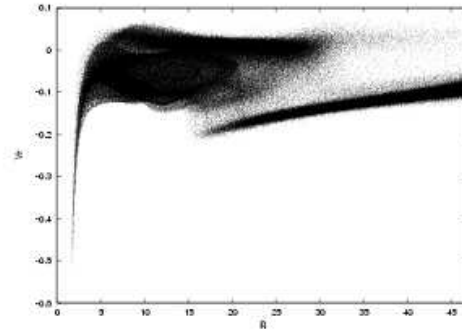


Figure 4.3 Radial speed versus R

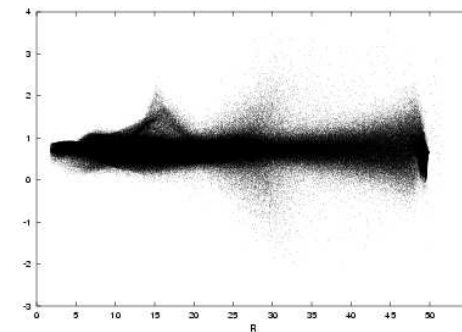


Figure 4.4 True angular momentum versus R

Panel 5. Simulation with  $f=0.4$

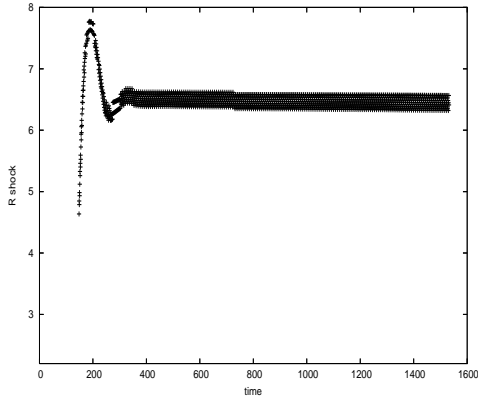


Figure 5.1 Shock position versus time

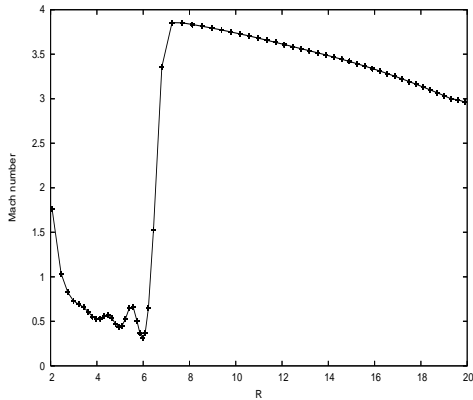


Figure 5.2 Radial Mach Number versus R

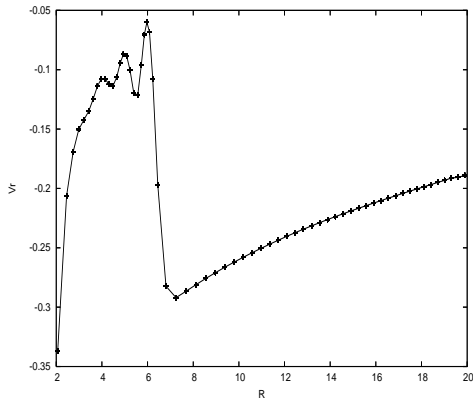


Figure 5.3 Radial speed versus R

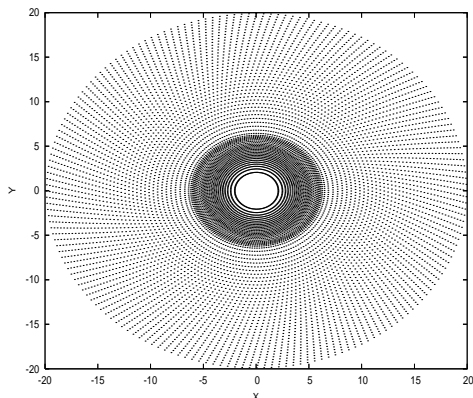


Figure 5.4 Particle distribution in the XY plane

## 6 ACKNOWLEDGEMENTS

The simulations have been performed at the italian CINECA center for super-computation. We are particularly grateful to Claudio Gheller for assistance in debugging the parallelized SPH code.

## REFERENCES

- Babul,A.; Ostriker Jeremiah P.; Meszaros,P., 1989, ApJ, 347, 59  
 Bondi, 1952, Month.Not. R. A. Soc., 112 , 195  
 S.K. Chakrabarti, Theory of Transonic Astrophysical Flows, World Scientific, Singapore, 1990  
 Chakrabarti, S. K. & Molteni, 1993, ApJ, 417, 671  
 S.K. Chakrabarti Observational Evidence for Black Holes in the Universe (Kluwer Academic, Dordrecht 1998)  
 Das S., Chattopadhyay I.& Chakrabarti, S. K., 2001, ApJ, 557, 983  
 Hawley, J. F., Wilson, J. R., Smarr, L. L., 1984, ApJ, 277, 296  
 Lucy, L.B., 1977, ApJ, 82, 1013  
 Molteni, D., Sponholz, H., Chakrabarti, S. K., 1996, ApJ, 457, 805  
 Molteni, D., Ryu, D., Chakrabarti, S. K. 1996, ApJ, 470, 460  
 Molteni, D.; Toth G.; Kuznetsov, O., 1999, ApJ , 516 , 411  
 Molteni, D.; Acharya, K.; Kuznetsov, O.; Bisikalo, D.; Chakrabarti, S. K. , 2001, ApJL, 563, L57  
 Monaghan J.J. , 1992, Ann. Rev. Astron. Astrophysics, 30, 543  
 Nakayama K., 1994, MNRAS, 270, 871  
 Paczyński, B., Wiita, P.J., 1980, A&A, 88, 23



**Table 1.**

	$r_i$	$v_{ri}$	$a_{ri}$	$\lambda$	H	f	$R_{shock}$	B
I	38	-0.076	0.069	1.625	16	0.0	5.76	0.0045
II	50	-0.072	0.058	1.65	20	0.1	6.32	0.003
III	50	-0.072	0.058	1.65	20	0.2	6.32	0.003
IV	50	-0.072	0.058	1.65	20	0.4	6.32	0.003